ELSEVIER

PII: S0032-3861(96)01065-8

Polymer Vol. 38 No. 18, pp. 4577–4585, 1997

0032-3861/97/$17.00+0.00

Analysis of polarized fluorescence intensity in an anisotropic polymer medium and its application to the orientation measurements for nylon 6 fibres

Shigemitsu Murase* and Matsuo Hirami
Research & Development Center, Unitika Ltd, Kyoto 611, Japan

and Yoshiyuki Nishio
Department of Material Systems Engineering, Tokyo University of Agriculture and Technology, Koganei, Tokyo 184, Japan

and Masahide Yamamoto
Department of Polymer Chemistry, Kyoto University, Kyoto 606-01, Japan
(Received 10 July 1996; revised 19 November 1996)

Polarized components of the fluorescence emitted from rod-like molecules (probes) oriented in a polymer medium are analysed theoretically. An 'envelope curve' of the polarized fluorescence intensity obtained in a rotating frame of two polaroids in the measuring system, is useful for characterizing the molecular orientation distribution. The model calculations are carried out in terms of three basic molecular orientation modes, i.e. uniaxial, random, and planar orientation modes. Generally, the envelope curve is affected by the birefringence due to the optical anisotropy of the polymer medium. In the highly uniaxial orientation mode, however, the shapes of the envelopes are scarcely distorted by the effect of birefringence. The fluorescence technique to measure envelope curves is employed to investigate the structural change of nylon 6 fibres upon drawing. The transformation of molecular orientation pattern in the non-crystalline phase of the drawn fibres is described satisfactorily by using a combination model composed of the three basic modes mentioned above, with their fractional parameters. A considerable portion of molecules in the amorphous regions may orient perpendicular to the draw direction, before the uniaxial orientation mode becomes predominant above *ca* 100% elongation. © 1997 Elsevier Science Ltd.

(Keywords: nylon 6 fibre; molecular orientation; optical anisotropy)

INTRODUCTION

Much effort has gone towards clarifying the molecular orientation characteristics of semi-crystalline polymers, which usually form not only a crystalline phase but also an amorphous phase in the solid state. If the degree of crystallinity and the orientation in the crystalline phase are both determined for a deformed polymer solid such as a fibre or a drawn film, the molecular orientation in the non-crystalline phase can also be deduced from an overall estimate of orientation. Stein and Norris[1] and Samuels[2] reported previously an optical method combined with a wide-angle X-ray diffractometry, for evaluating the degree of molecular orientation in the non-crystalline regions; subtraction of the contribution of the crystalline orientation from the total birefringence is an essential point of the evaluation. Thus, the combined use of two different techniques is often of benefit to study the molecular orientation of semi-crystalline polymers.

Various techniques have been established to estimate the molecular orientation in polymer solids, including X-ray diffraction[3–8], sonic velocity measurements[4], nuclear magnetic resonance[6], Raman spectroscopy[7,9,10], ultraviolet–visible u.v.–vis and infra-red absorption dichroism[11], birefringence[12–14] and fluorescence polarization measurements[15–17]. Among these, u.v.–vis absorption dichroism and fluorescence polarization measurements provide information of the non-crystalline molecular orientation without the aid of other measurements. Especially, the fluorescence method is superior to absorption dichroism, because the former enables us to estimate the fourth-order moment of the orientation distribution. The application of polarized fluorescence to the measurement of molecular orientation in polymers was first explored by Nishijima and coworkers[18–20]. Afterwards, Ward and coworkers[21,22], Hibi *et al.*[23], and Nishio and coworkers[24,25], have investigated in detail the orientation behaviour of polymer films on stretching, by this method. Most of the studies have been conducted with fluorescent probe molecules incorporated into the polymer solids in the solution casting or melt-extrusion process; whereupon the probe molecules were reasonably assumed to be accommodated in the amorphous regions rather than in the crystals of the polymers[18,20,26,27].

* To whom correspondence should be addressed

We examined the molecular orientation of nylon 6 melt-spun fibres by the fluorescence method. The fibres contain an adequate amount of fluorescent molecules as the orientation probe in the non-crystalline regions. We measured the 'envelope curve' of polarized fluorescence intensity, which was obtained by rotating a polarizer and an analyser synchronously in the optical apparatus employed. The measurements were compared with the corresponding curves calculated with a transformation model composed of a mixture of three orientation modes. We also discussed the effect of the optical birefringence of the polymer matrix in which fluorescent molecules were dispersed.

THEORY

The selective light absorption of fluorescent molecules and the polarization characteristics of the emitted fluorescence are, in the simplest case, explicable in terms of an oscillator model: when a fluorescent molecule having an absorbing oscillator **A** is excited by polarized light with an electric vector $\mathbf{P_1}$, the probability of excitation, i_a, is proportional to the square of a scalar product of **A** and $\mathbf{P_1}$, i.e.

$$i_a \propto (\mathbf{A} \cdot \mathbf{P_1})^2 = \cos^2 \alpha$$

where α is an angle between the two vectors. Subsequently, if the fluorescence light emitted from an oscillator **F** of the excited molecule is detected as a component with its electric vector $\mathbf{P_2}$, the probability of detection, i_f, can also be represented as

$$i_f \propto (\mathbf{F} \cdot \mathbf{P_2})^2 = \cos^2 \beta$$

where β is an angle between **F** and $\mathbf{P_2}$. In the present treatment, we assume that both the absorbing oscillator and the emitting oscillator coincide with a single axis **M** of the fluorescent molecule as a rod-like probe of orientation, as shown in *Figure 1*.

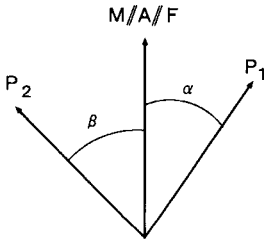

Figure 1 Angular relationships between the molecular axis (**M**) of a fluorescent probe and the electric vectors of exciting polarized light ($\mathbf{P_1}$) and detected fluorescence light ($\mathbf{P_2}$). Both absorbing and emitting oscillators, **A** and **F**, respectively, are assumed to coincide with the **M**-axis in the present treatment

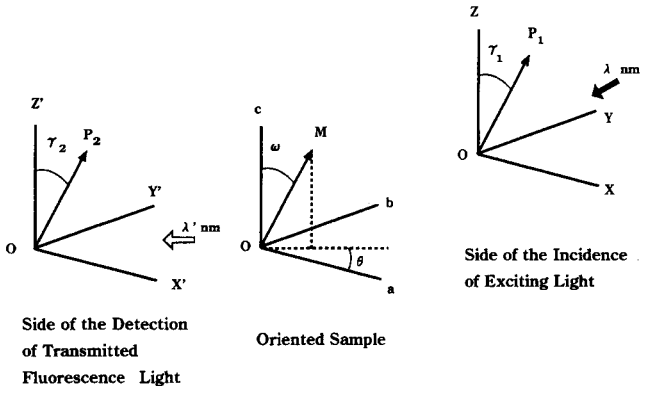

Figure 2 Three coordinate systems defined in an apparatus for measuring the polarized fluorescence intensity: *0-abc* is a coordinate system fixed to a polymer sample, and *0-XYZ* and *0-X'Y'Z'* are optical coordinate systems situated, respectively, on the incident side of the exciting light beam and on the detection side of the emitted fluorescence light

Figure 2 shows an arrangement of three coordinate systems: *0-abc* is a coordinate system fixed to a polymer sample, and the other optical coordinate systems *0-XYZ* and *0-X'Y'Z'* are spaced, respectively, on the side of the incidence of exciting light of a wavelength λ and on the side of the detection of fluorescence light of a wavelength $\lambda'(> \lambda)$. The orientation of the molecular axis **M** of a fluorescent probe is specified by a set of polar and azimuthal angles (ω, θ) in the sample coordinate system *0-abc*. Angles γ_1 and γ_2 specify the alignments of the transmission axis of a polarizer ($\mathbf{P_1}$) and that of an analyser ($\mathbf{P_2}$), both rotatable in the *XZ*- and *X'Z'*-plane, respectively. Then, the overall intensity of the polarized component of the fluorescence obtained from the oriented sample can be written as follows.

$$I(\gamma_1, \gamma_2) = \int_0^{2\pi} \int_0^{\pi} i_a \cdot i_f \cdot \Omega(\omega, \theta) \cdot \sin\omega \cdot d\omega \cdot d\theta \quad (1)$$

$$\text{with } i_a = k \cdot \cos^2 \alpha \quad (2)$$

$$i_f = \phi \cdot \cos^2 \beta \quad (3)$$

where $\Omega(\omega, \theta)$ is a normalized function representing the molecular orientation distribution in the *0-abc* system, and k and ϕ are proportional constants referring to the efficiency of the absorption and that of emission, respectively, of the fluorescent probe used.

The illustrations given in *Figure 3* make clearer the angular alignments of the vectors, **M**, $\mathbf{P_1}$ and $\mathbf{P_2}$ in the three coordinate systems defined above. In the coordinate arrangement adopted here, the principal axes *a*, *b*, and *c* in the sample coordinate system are laid along the directions of the *X*-, *Y*- and *Z*-axis, respectively, in the optical coordinate system *0-XYZ* and the *Z*-axis of the latter framework makes an angle ψ with the *Z'*-axis in the coordinate system *0-X'Y'Z'*, as shown in *Figure 3C*. Using a theorem taken from spherical trigonometry, the following relationships hold among the orientation angles specified in *Figure 3*.

$$\cos\alpha = \cos\omega \cdot \cos\gamma_1 + \sin\omega \cdot \cos\theta \cdot \sin\gamma_1 \quad (4)$$

$$\cos\beta = \cos\omega' \cdot \cos\gamma_2 + \sin\omega' \cdot \cos\theta' \cdot \sin\gamma_2 \quad (5a)$$

$$= (\cos\omega \cdot \cos\psi - \sin\omega \cdot \sin\theta \cdot \sin\psi) \cdot \cos\gamma_2 + \sin\omega \cdot \cos\theta \cdot \sin\gamma_2 \quad (5b)$$

As a measuring condition, let the polarizer and analyser be rotated synchronously at a different speed, i.e. let the angles γ_1 and γ_2 vary with time (t_r) as

$$\gamma_1 = \omega_1 t_r \quad (6)$$

$$\gamma_2 = \omega_2 t_r \quad (7)$$

where ω_1 and ω_2 are the angular velocities of the rotating polarizer and of the analyser. In this case, the excitation probability i_a and the detection probability i_f, given

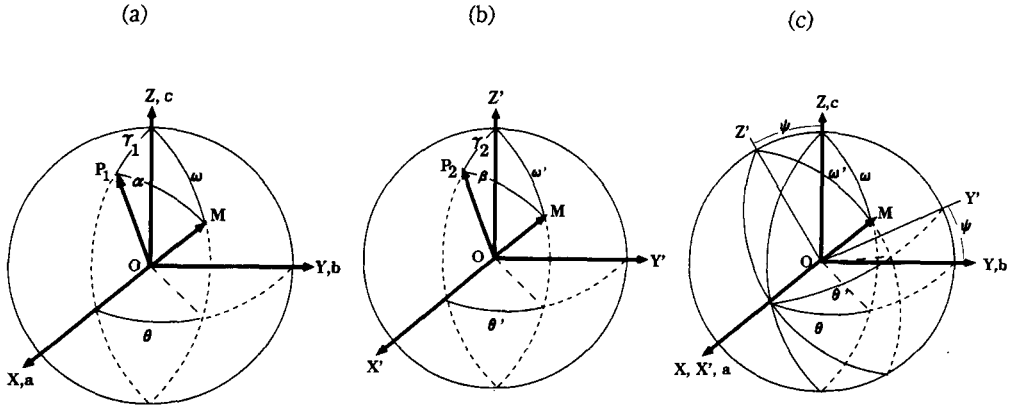

Figure 3 Relationships in spatial arrangement between the coordinate systems *0-abc*, *0-XYZ*, and *0-X'Y'Z'*, and specifications of the orientation of the molecular axis (**M**) and transmission axes of polarizer ($\mathbf{P}_1$) and analyzer ($\mathbf{P}_2$) with respect to the respective coordinate systems

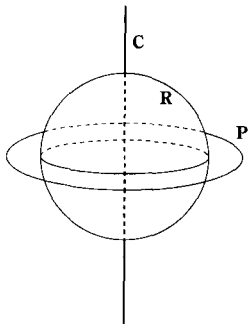

Figure 4 Schematic representation of three basic modes of molecular orientation: *c*-axis perfect uniaxial (*C*), three-dimensional random (*R*), and *ab*-planar orientation (*P*) modes

Table 1 Three basic modes of molecular orientation for deformed polymer samples

Orientation mode	Distribution function[a], $\Omega(\omega,\theta)$
c-Axis perfect uniaxial	$\delta(\omega-0)$
Random	$1/4\pi$
ab-Planar	$\delta(\omega-2\pi)$

[a] δ denotes a Dirac delta function

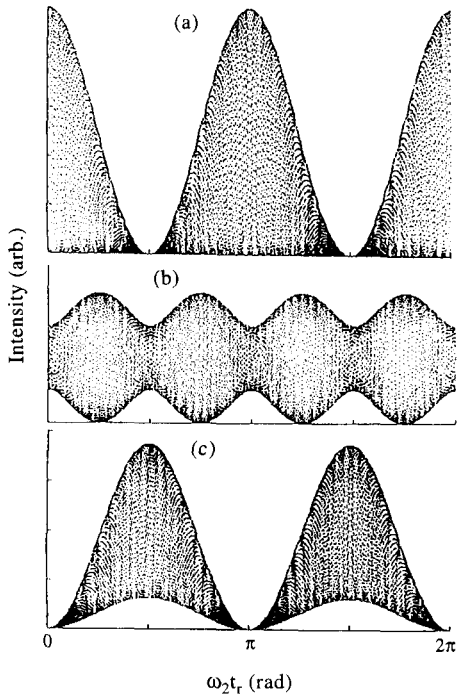

Figure 5 Envelope curves corresponding to the three basic orientation modes: (a) *c*-axis perfect uniaxial; (b) random; (c) *ab*-planar orientation

equations (2) and (3), respectively, can be rewritten by using equations (4)–(7), as follows:

$$i_a = k[\cos\omega \cdot \cos(\omega_1 t_r) + \sin\omega \cdot \cos\theta \cdot \sin(\omega_1 t_r)]^2 \quad (8)$$

$$i_f = \phi[(\cos\omega \cdot \cos\psi - \sin\omega \cdot \sin\theta \cdot \sin\psi) \cdot \cos(\omega_2 t_r) + \sin\omega \cdot \cos\theta \cdot \sin(\omega_2 t_r)]^2 \quad (9)$$

In such continuous measurements at a constant ratio of ω_1/ω_2, the observed intensity of fluorescence, $I(\gamma_1,\gamma_2)$, should vary periodically as a function of $\omega_2 t_r$. The variation would yield a pair of envelope curves reflecting the type of molecular orientation distribution in the sample.

Now, let us exemplify the construction of such envelope curves in terms of three basic modes of molecular orientation. *Figure 4* shows the three modes schematically[19]: (a) *c*-axis perfect uniaxial orientation; (b) three-dimensional random orientation; (c) *ab*-planar orientation. In mode (a), all the molecules (probes) are oriented along the *c*-axis (stretching axis) of the specimen, while mode (c) denotes that the molecules lie perpendicular to the *c*-axis with no preferred orientation in the *ab*-plane.

Table 1 summarizes the explicit forms of the distribution function $\Omega(\omega,\theta)$ representing the basic orientation modes. By substituting equations (8) and (9) into equation (1), and using the respective form of $\Omega(\omega,\theta)$, the intensity of polarized fluorescence can be expressed as follows:

(a) *c*-axis perfect uniaxial orientation

$$I_C(\omega_2 t_r) = k\phi \cdot \cos^2(\omega_1 t_r) \cdot \cos^2(\omega_2 t_r) \quad (10)$$

(b) random orientation

$$I_R(\omega_2 t_r = k\phi\{(\sqrt{2}\sin(\omega_1 t_r) \cdot \sin(\omega_2 t_r) + \cos(\omega_1 t_r) + \cos(\omega_2 t_r))^2 + 1\}/15 \quad (11)$$

(c) *ab*-planar orientation

$$I_P(\omega_2 t_r) = k\phi[\sin^2(\omega_1 t_r) \cdot \{5\sin^2(\omega_2 t_r) + 1\}]/16 \quad (12)$$

For the above formulations, the angle ψ appearing in equations (8) and (9) was set equal to $\pi/4$, this being the condition actually adopted in the fluorescence measurements.

Figure 5 illustrates three types of envelope curves corresponding to the orientation modes (a)–(c), constructed through calculations taken as $\omega_1/\omega_2 = 225$, with equations (10)–(12).

As discussed later, experimental data are analysed by using a model composed of the three basic orientation modes mentioned above. In this combination model, the contributions of the *c*-axis perfect uniaxial, random, and *ab*-planar orientation modes are indicated by fractional parameters C, R, and P, respectively, so that the equation for the polarized fluorescence intensity is represented as

$$I(\omega_2 t_r) = C \cdot I_C(\omega_2 t_r) + R \cdot I_R(\omega_2 t_r) + P \cdot I_P(\omega_2 t_r) \quad (13)$$

$$\text{with } C + R + P = 1 \quad (14)$$

Figure 6 shows an example of the envelope curves, depicted for a parameter setting: $C = 0.5$, $R = 0.25$ and $P = 0.25$.

In the above treatment, all the calculations were carried out for the oriented system of fluorescent molecules dispersed in an 'isotropic' medium. However, deformed polymer specimens are generally optically anisotropic. For such optically anisotropic systems, we must take into account a 'birefringence effect' in the analysis of polarized fluorescence intensity.

When an incident exciting light with an electric vector $\mathbf{P_1}$ enters an anisotropic medium, it propagates as two components with mutually different vibration axes and velocities. Let E_Z and E_X be the electric fields of the two components of the exciting light, just absorbed along the oscillator of a fluorescent molecule which is located at a distance L from the surface of the specimen of thickness D. For the same angular alignments as specified in *Figure 3*, E_Z and E_X can be written as follows:

$$E_z = I_z \cdot \sin(2\pi t/T)$$
$$= \cos\omega \cdot \cos(\omega_1 t_r) \cdot \sin(2\pi t/T) \quad (15a)$$

$$E_x = I_x \cdot \sin(2\pi t/T - \delta_L)$$
$$= \sin\omega \cdot \cos\theta \cdot \sin(\omega_1 t_r) \cdot \sin(2\pi t/T - \delta_L) \quad (15b)$$

In these equations, T is a temporal period of the exciting light wave and δ_L is a phase difference given by

$$\delta_L = 2\pi \cdot \Delta n \cdot L/\lambda \quad (16)$$

where $\Delta n (= n_c - n_a)$ is the birefringence of the medium having the principal refractive indices n_a, n_b and n_c. In this situation, the absorption intensity per unit probe, i.e. the excitation probability i_a, can be expressed as follows.

$$i_a = k(I_z^2 + I_x^2 + 2 \cdot I_z \cdot I_x \cdot \cos\delta_L)$$
$$= k[\cos^2\omega \cdot \cos^2(\omega_1 t_r) + \sin^2\omega \cdot \cos^2\theta \cdot \sin^2(\omega_1 t_r)$$
$$+ 2\sin\omega \cdot \cos\omega \cdot \cos\theta \cdot \sin(\omega_1 t_r) \cdot \cos(\omega_1 t_r)$$
$$\cdot \cos\delta_L] \quad (17)$$

Similarly, the fluorescence light emitted from the excited molecule is also affected by the optical anisotropy of the medium. When we observe the fluorescence light through an analyzer ($\mathbf{P_2}$) in the optical arrangement shown in *Figures 2* and *3*, the following two components may be taken into consideration in the intensity measurement.

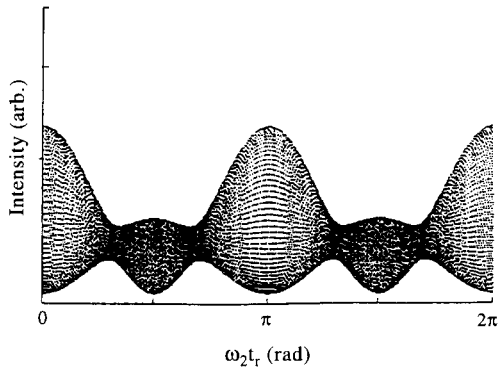

Figure 6 Envelope curves according to a model composed of a mixture of the three basic orientation modes, calculated by equation (13) with $C = 0.5$, $R = 0.25$, and $P = 0.25$

$$E_{Z'} = I_{z'} \cdot \sin(2\pi t/T')$$
$$= (\cos\omega \cdot \cos\psi - \sin\omega \cdot \sin\theta \cdot \sin\psi)$$
$$\cdot \cos(\omega_2 t_r) \cdot \sin(2\pi t/T') \quad (18a)$$

$$E_{x'} = I_{x'} \cdot \sin(2\pi t/T' - \delta_{L'})$$
$$= \sin\omega \cdot \cos\theta \cdot \sin(\omega_2 t_r)$$
$$\cdot \sin(2\pi t/T' - \delta_{L'}) \quad (18b)$$

where T' is a temporal period of the fluorescence light wave, and $\delta_{L'}$ is a phase difference between the two components and given by

$$\delta_{L'} = 2\pi \cdot \Delta n' \cdot (D - L)/\lambda' \quad (19)$$

$\Delta n'$ is the birefringence for the wavelength λ' and $\Delta n' \simeq \Delta n$ when the effect of wavelength distribution is substantially negligible. Thus the fluorescence detection probability per unit probe i_f can also be represented as

$$i_f = \phi(I_{z'}^2 + I_{x'}^2 + 2I_{z'} \cdot I_{x'} \cdot \cos\delta_{L'})$$
$$= \phi[(\cos\omega \cdot \cos\psi - \sin\omega \cdot \sin\theta \cdot \sin\psi)^2$$
$$\cdot \cos^2(\omega_2 t_r) + \sin^2\omega \cdot \cos^2\theta \cdot \sin^2(\omega_2 t_r)$$
$$+ 2\sin\omega \cdot \cos\theta \cdot (\cos\omega \cdot \cos\psi - \sin\omega \cdot \sin\theta \cdot \sin\psi)$$
$$\cdot \sin(\omega_2 t_r) \cdot \cos(\omega_2 t_r) \cdot \cos\delta_{L'}] \quad (20)$$

The total fluorescence intensity obtained from the anisotropic system, in which fluorescent probes are dispersed so as to obey the orientation distribution function $\Omega(\omega, \theta)$, can be calculated from the following equation with equations (17) and (20).

$$I(\gamma_1, \gamma_2) = \int_0^D \int_0^{2\pi} \int_0^{\pi} i_a \cdot i_f \cdot \Omega(\omega, \theta) \cdot \sin\omega \cdot d\omega \cdot d\theta \cdot dL/D \quad (21)$$

If $\delta_L = \delta_{L'} = 0$, i.e. the medium is isotropic, equations (17) and (20) coincide with equations (8) and (9), respectively.

Again, let us consider the three orientation modes listed in *Table 1*, but in the optically anisotropic medium. Using equation (21) with equations (17) and (20) (taken as $\psi = \pi/4$), we have the following simplified equations of the polarized fluorescence intensity for the respective modes.

(a) *c*-axis perfect uniaxial orientation

$$I_C(\omega_2 t_r) = k \cdot \phi \cdot \cos^2(\omega_1 t_r) \cdot \cos^2(\omega_2 t_r) \quad (22)$$

(b) random orientation

$$I_R(\omega_2 t_r) = k \cdot \phi\{1 + \cos^2(\omega_1 t_r) \cdot \cos^2(\omega_2 t_r) + 2\sin^2(\omega_1 t_r) \cdot \sin^2(\omega_2 t_r) + \sqrt{2}Q \cdot \sin(\omega_1 t_r) \cdot \cos(\omega_1 t_r) \cdot \sin(\omega_2 t_r) \cdot \cos(\omega_2 t_r)\}/15 \quad (23)$$

(c) *ab*-planar orientation

$$I_P(\omega_2 t_r) = k \cdot \phi[\sin^2(\omega_1 t_r) \cdot \{5\sin^2(\omega_2 t_r) + 1\}]/16 \quad (24)$$

A notation Q, appearing in equation (23), is set as

$$Q = \cos\delta'\left\{\frac{\sin(\delta+\delta')}{\delta+\delta'} + \frac{\sin(\delta-\delta')}{\delta-\delta'}\right\} + \sin\delta'\left\{\frac{1-\cos(\delta+\delta')}{\delta+\delta'} + \frac{1-\cos(\delta-\delta')}{\delta-\delta'}\right\} \quad (25)$$

where

$$\delta = 2\pi\Delta n \cdot D/\lambda = 2\pi\Gamma/\lambda \quad (26a)$$

$$\delta' = 2\pi\Delta n' \cdot D/\lambda' = 2\pi\Gamma'/\lambda' \quad (26b)$$

Thus Q is a function of a so-called optical retardation (Γ or Γ') of the sample medium.

From these calculations, it is evident that the polarized fluorescence intensity for the random orientation mode (b) is affected by the birefringence of the anisotropic medium. In contrast, when the molecular orientation mode is perfectly uniaxial (a) or *ab*-planar (c), the optical anisotropy of the sample medium is ineffective to the quantification of polarized fluorescence intensity.

Figure 7 shows two variant envelope curves of the polarized fluorescence intensity for the random orientation mode, making a comparison between the two extreme cases: $\Gamma = 0$ nm and $\Gamma = 2000$ nm, representing whether the medium is isotropic or highly birefringent. We can see a large difference in oscillation manner between the two envelope curves; however, every $(\pi/2)$ s of $\omega_2 t_r$, the fluorescence intensity is free from the birefringence effect in spite of the optical anisotropy of the medium.

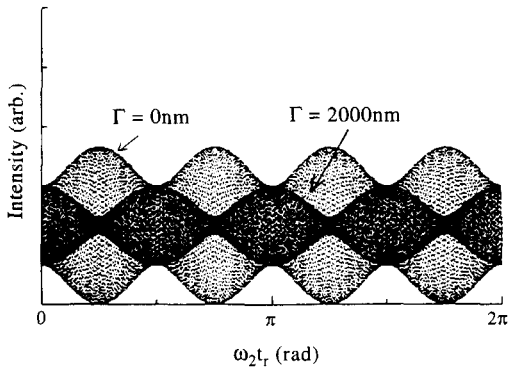

Figure 7 Comparison of envelope curves for the random orientation mode between the two cases; $\Gamma = 0$ nm and $\Gamma = 2000$ nm

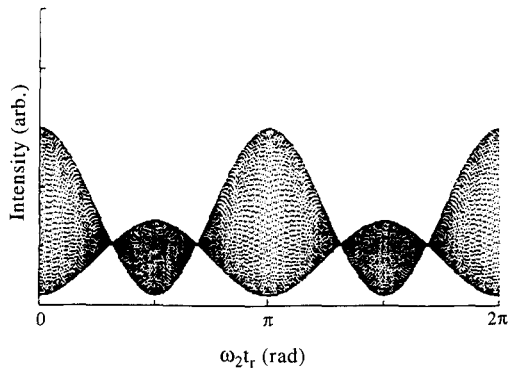

Figure 8 Envelope curves according to a model composed of three basic orientation modes, calculated by a linear combination of equations (22)–(24) with $C = 0.5$, $R = 0.25$, $P = 0.25$, and $\Gamma = 2000$ nm

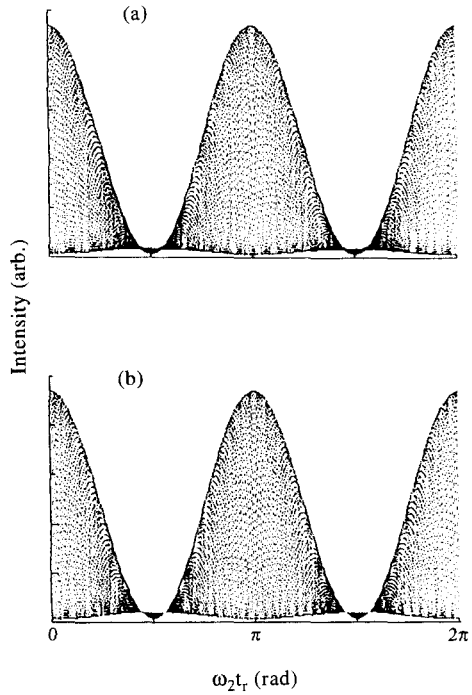

Figure 9 Envelope curves calculated by a linear combination of equations (22)–(24) with $C = 0.9$, $R = 0.1$, $P = 0$, and $\Gamma = 0$ nm (a) or 2000 nm (b)

For the model composed of the basic three modes of molecular orientation, the fluorescence intensity is expressed by a linear combination of equations (22)–(24), i.e. as equation (13) with the fractional parameters C, R, and P. In the practical analysis of observed data, the three parameters were pro-rated with a ratio of the maximum to the minimum intensity at $\omega_2 t_r = \pi/2$ and a similar intensity ratio at $\omega_2 t_r = 0$ in the envelope curves.

Figure 8 depicts an example of typical envelope curves, calculated according to the combination model with the following values: $C = 0.5$, $P = R = 0.25$, and $\Gamma(\simeq \Gamma') = 2000$ nm. The envelopes differ in shape from those given in *Figure 6* in the angular range of $(\pi - 1)/2 \leqq \omega_2 t_r \leqq (\pi + 1)/2$. *Figure 9* shows other examples, calculated with $C = 0.9$, $R = 0.1$, and $P = 0$ in two cases: (a) $\Gamma = 0$ nm; (b) $\Gamma = 2000$ nm. There is no appreciable difference

between the two examples of envelope curves. In fact, after repeated calculation, we confirmed that the effect of birefringence can be neglected as far as the *c*-axis perfect uniaxial and/or *ab*-planar mode is dominant in the combination model. In a process of the industrial fibre production, solution- or melt-spun fibres are drawn along the fibre axis, and consequently they show a nearly uniaxial orientation. Therefore, at a stage of higher elongation, the effect of birefringence may be virtually negligible.

EXPERIMENTAL

Samples

The fluorescent molecule used as a probe for orientation estimation was a stilbene derivative, Whitex RP (Sumitomo Chemical Co.), whose chemical structure is shown below:

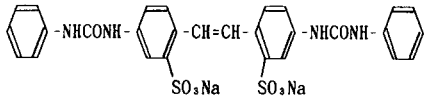

The intrinsic viscosity $[\eta]$ of the nylon 6 used in this study was 1.164, and its number-average molecular weight, M_n, was estimated to be 16990 by use of a relationship presented by Matthes[28]. Fibre samples containing the fluorescent additive at a concentration of 0.01 wt% were prepared by melt-spinning and winding at a take-up speed of 800 m min^{-1}; the denier of the filament was 400, and the filament count was 24. The as-spun fibres were then drawn at 90°C at different ratios ranging from 1.5 to 4.0, followed by rapid cooling to room temperature (20°C). These samples were stored at 20°C and 65% relative humidity for more than 24 h before use, and the orientation measurements were carried out under the same conditions.

Structural characterization

Density measurements were carried out with a gradient column, in which the solvent used was a mixture of tetrachloroethane and toluene at 25°C.

Wide-angle X-ray diffraction (WAXD) measurements were made by using a Rigaku Denki model RAD-rB with Nickel-filtered Cu–K_α radiation of 50 kV and 200 mA. The crystalline orientation function (f_c) was determined through assessment of the half-height width ($H_{1/2}$) of intensity profile for the (200) and (002/202) reflection arcs coming from the α-form crystal[29], by using the following equation:

$$f_c = (3\langle\cos^2\omega\rangle_c - 1)/2 = (180 - H_{1/2})/180 \quad (27)$$

In addition, the crystal perfection index (CPI) was estimated from observed values of the *d*-spacings of the (200) and (002)/(202) planes in the α-form crystalline domains, by utilizing the following equation[30]:

$$\mathrm{CPI} = \{(d(200)/d(002/202) - 1)/0.1935\} \times 100 \quad (28)$$

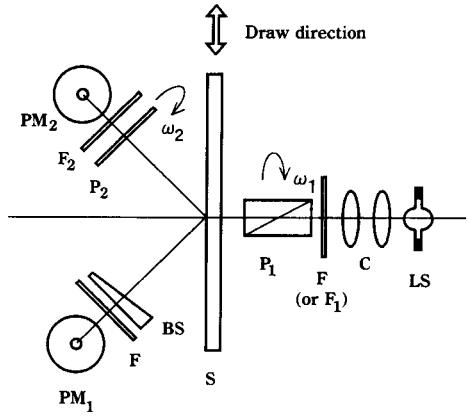

Figure 10 Diagram of the optical apparatus used for measuring the polarized fluorescence intensity and the birefringence of polymer samples: LS, light source (mercury arc lamp); C, collimating lens system; F and F_1, monochromatic filters; P_1, rotatable polarizer; S, oriented sample; P_2, rotatable analyzer; F_2, cut-off filter; PM_1 and PM_2, photomultipliers; BS, Babinet compensator

Birefringence

The apparatus used for birefringence measurements is shown schematically in *Figure 10*. Light from a source (a mercury arc lamp), LS, was rendered parallel by a collimating lens system, C. The wavelength of the incident light was 546 nm through a monochromatic filter, F, and it was lineally polarized by a polarizer, P_1. The monochromatic light beam then fell on a polymer sample, S. The retardation of the sample was measured by a Babinet compensator, BS, with a servo motor, followed by the detection of the transmitted light by a photomultiplier, PM_1, through the same monochromatic filter as used in the incident side.

Measurements of envelope curves

The measurements of the envelope curves of polarized fluorescence intensity were carried out with the same apparatus as employed for the birefringence measurements, as is also summarized schematically in *Figure 10*. The optical coordinate systems required were already defined in *Figures 2* and *3*. The wavelength of the exciting light was 365 nm through a monochromatic filter, F_1. The polarized components of fluorescence intensity were measured by a photomultiplier, PM_2, through an analyser, P_2, and a cut-off filter, F_2, with a cut-off wavelength of 420 nm. The angle, ψ, defined as $\angle ZOZ'$ in *Figure 3C* was set equal to $\pi/4$, and the angular velocities of the rotating vector $\mathbf{P_1}$ and that of $\mathbf{P_2}$ were $\omega_1 = 30\pi\,\mathrm{s}^{-1}$ (900 rpm) and $\omega_2 = 2\pi/15\,\mathrm{s}^{-1}$ (4 rpm), respectively.

RESULTS AND DISCUSSION

Characterization of crystalline phase

The data of the crystalline structure and orientation of crystalline phase for drawn fibres of nylon 6, obtained by WAXD and density measurements, are listed in *Table 2*. Nylon 6 produces two types of crystal, α-form[29] and γ-form[31]. The α-form crystal is made up of an extended chain structure with hydrogen bondings of –CO···NH– between anti-parallel chains, while the γ-form crystal has a structure in which the hydrogen bondings are formed between parallel chains and the repeating unit is significantly short. The α-form crystal is more stable

Table 2 Structural data for Nylon 6 crystals in the drawn fibres

Draw ratio	Degree of crystallinity (%)		f_c	Crystal perfection index	$\frac{I_{(002,202)}}{I_{(200)}}$
	α-form	γ-form			
2.0	27.0	3.6	0.826	–	
3.0	30.7	1.2	0.862	59	1.08
3.5	31.7	0.5	0.881	76	1.11
4.0	31.8	0.8	0.898	89	1.12

than the γ-form crystal. By drawing or heat treatment, the γ-form crystal changes easily to the α-form crystal[32].

It is possible to determine the proportion of the α-form crystallinity to the γ-form crystallinity present in a nylon 6 sample, via a certain chemical treatment; viz. the α-form crystal is easily converted into the γ-form crystal by the treatment with an aqueous iodide–potassium iodide solution and then by washing with a sodium thiosulfate solution. The details of the procedure will be reported elsewhere[33]. The crystallinity data for the nylon 6 fibres prepared in this study are shown in *Table 2*; the degree of α-form crystallinity is around 30% (per unit weight of sample), whereas the γ-form crystallinity is much less than a few per cent. Thus the α-form dominates the crystalline phase in the nylon 6 fibres.

Table 2 also compiles the data of CPI defined by equation (28), together with values of the ratio of the intensity of the (002/202) diffraction ($I_{(002/202)}$) to that of the (200) diffraction ($I_{(200)}$). Both the CPI and the WAXD intensity ratio increase with an increase in the extent of drawing. This observation can be interpreted as a consequence of the enhancement of hydrogen bondings formed in the (002) planes. Such an intermolecular rearrangement accompanying the drawing would be sufficient to give rise to the growth in size and the increase in ordering of the α-form crystals of nylon 6.

The crystalline orientation function, f_c, was more than 0.86 at a draw ratio of 3.0 and approximately 0.90 at a draw ratio of 4.0. Further drawing of fibres was possible; however, the increment of the f_c value was quite small.

Amorphous orientation

The amorphous orientation function, f_a, was calculated by the following equation[1]:

$$\Delta n = \Delta n_{c0} \cdot f_c \cdot X_c + \Delta n_{a0} \cdot f_a \cdot (1 - X_c) \qquad (29)$$

where Δn is the birefringence of a deformed polymer sample and X_c denotes the degree of crystallinity. Δn_{c0} and Δn_{a0} are the intrinsic birefringences of the crystalline and non-crystalline regions, respectively. In the present study, we used the following literature data for nylon 6: $\Delta n_{c0} = 0.094$[34] and $\Delta n_{a0} = 0.078$[35]. The Δn_{c0} value adopted is given for the α-form crystal of nylon 6 and, needless to say, different from that for the γ-form crystal. As shown above, however, the α-form crystal generated exclusively and the proportion of the γ-form crystalline domains was usually less than 1% in the nylon 6 fibres prepared.

In *Figure 11*, the crystalline and amorphous orientation functions are plotted against the draw ratios of the fibres. Concerning the crystalline orientation, the increase of the draw ratio from 2 to 4 elicited only an 8.5% increase in the value of f_c; however, it has a high

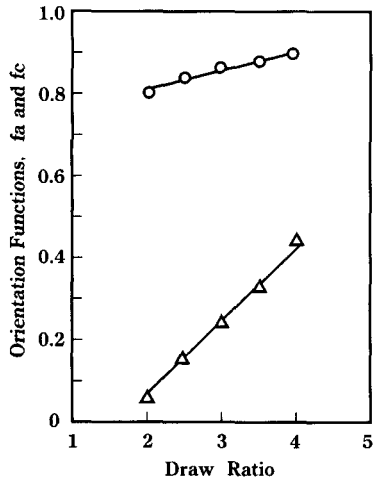

Figure 11 Crystalline and amorphous orientation functions, f_c and f_a, respectively, plotted against draw ratio, estimated for nylon 6 fibres by the combined use of the WAXD and birefringence measurements

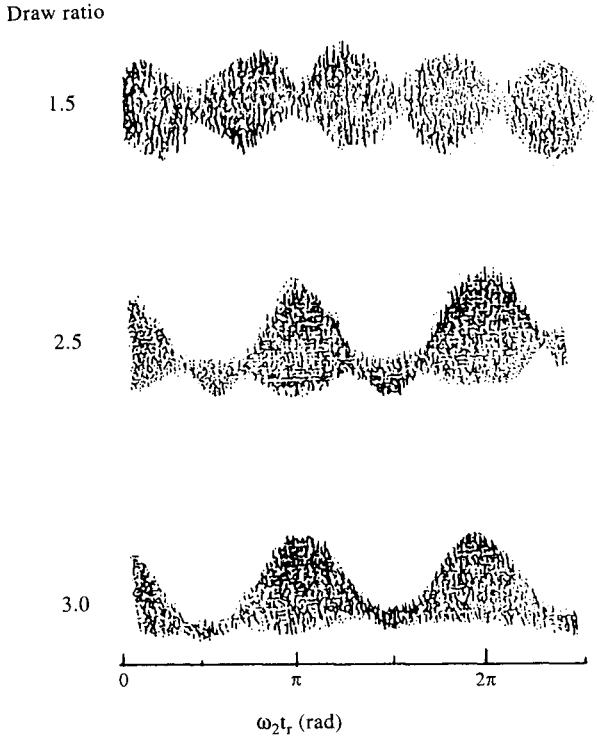

Figure 12 Typical examples of envelope curves observed for drawn nylon 6 fibres

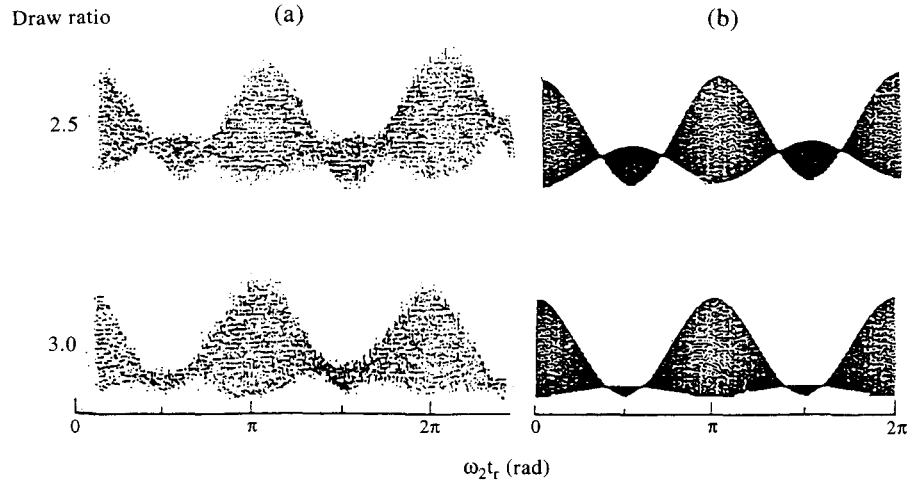

Figure 13 Comparison of (a) observed envelope curves with (b) calculated ones, for two drawn samples of nylon 6 fibre which showed the optical anisotropy of $\Gamma = 1850$ nm (upper) and 2040 nm (lower)

value (~0.82) even at the lower draw ratio. On the other hand, in the corresponding range of elongation, the amorphous orientation function, f_a, increased more markedly with the increase of the draw ratio. Thus, f_a depended more strongly on the draw ratio, compared with the function f_c, in the case of stretching of nylon 6 fibres. However, the value of f_a was estimated from equation (29) indirectly, i.e. by subtracting the contribution of the crystalline orientation from the total birefringence.

Next, the amorphous orientation behaviour of nylon 6 fibres is discussed based on the measurements of envelope curves of fluorescence intensity.

Figure 12 shows selected data of the observed envelope curves. The shape of the envelopes changes systematically with the increase of the draw ratio. At draw ratios lower than 2.0, the envelope curves appear to make a pair of sinusoidal trajectories, with almost the same period and amplitude of variation. When the draw ratio becomes higher than 2.0, the intensity at around $\pi/2$ of $\omega_2 t_r$ tends to be lowered, and, consequently, the shape of the envelopes becomes completely different from those obtained at the lower draw ratio.

Figure 13 shows a comparison of the observed envelope curves with theoretical ones calculated in terms of a linear combination of equations (22)–(24). In the two examples, the theoretical envelope curves (*Figure 13b*) were obtained by taking into account the birefringence effect, for the following sets of the fractional parameters: $C = 0.65$, $R = 0.03$, and $P = 0.32$ (upper); $C = 0.87$, $R = 0.04$, and $P = 0.09$ (lower). The respective envelopes are in good agreement with the corresponding observed ones shown in *Figure 13a*.

Figure 14 shows the draw ratio dependence of the fractions of the *c*-axis perfect uniaxial, three-dimensional random, and *ab*-planar orientation modes. As the draw ratio was increased to 2.0, both the fraction of the uniaxial orientation and that of the planar orientation increased to almost the same value, while the fraction of the random orientation decreased abruptly. The prevalence of such a planar orientation mode at an early stage of the drawing of nylon 6 fibres is quite interesting. Analogous orientation behaviour has been pointed out by other investigators who focused on lamellar crystallites as the orientation unit. Katayama *et al.*[36] reported a

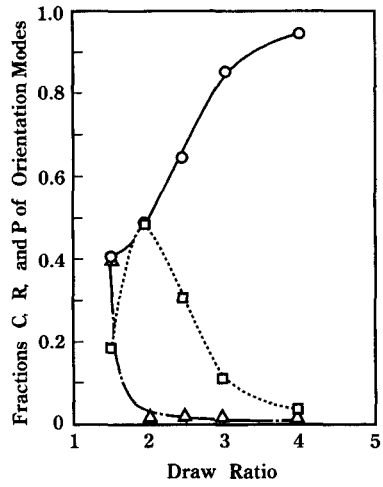

Figure 14 Draw ratio dependence of the fractions of three basic molecular orientation modes: ○, fraction (*C*) of the *c*-axis perfect uniaxial orientation; △, fraction (*R*) of the random orientation; □, fraction (*P*) of the *ab*-planar orientation

planar orientation for polypropylene fibres in which crystalline lamellae tended to be aligned perpendicular to the fibre axis. Sakaoku *et al.*[37] also reported, for nylon 6 fibres, that the lamellae were arranged almost perpendicular to the fibre axis at lower draw ratios. Our finding of a similar orientation mode for molecules in the non-crystalline phase may be of significance for further elucidation of the development of supramolecular architectures in drawn synthetic fibres.

After the draw ratio exceeded 2.0, the random orientation mode was almost undiscernible, and instead, the fraction of the *c*-axis uniaxial orientation mode increased conspicuously with the extent of drawing and the fraction of the *ab*-planar orientation mode decreased rapidly. In the corresponding range of elongation, the molecular orientation function, f_c, defined for the crystalline phase, also increased monotonically (see *Figure 11*); however, the degree of increment was much smaller than that in the amorphous orientation function, f_a, as has already been inferred by the combined use of the WAXD and birefringence measurements.

Thus, we successfully described a transformation mechanism of the three-dimensional orientation distribution

pattern in nylon 6 fibres on drawing, by employing the fluorescence method utilizing the envelope curves. Decidedly, this method supplements effectively the popular characterization of oriented polymers, performed with the averaged degree of molecular orientation which is commonly evaluated by the WAXD and/or birefringence measurements.

In the present paper, the full analysis of fluorescence data was restricted to the nylon 6 fibres deformed at 90°C to a draw ratio not exceeding 4.5. These samples gave a relatively small value of density (1.13–1.135) and therefore exhibited a rather lower crystallinity (26–31%). In a case where more highly crystalline (e.g. $\geq 45\%$) or heavily opaque polymer samples are used, however, attention should be paid to an additional effect, i.e. fluorescence depolarization due to light scattering[16,38], which may not be negligible, as well as the birefringence effect for precise estimation of the molecular orientation pattern by the fluorescence method.

SUMMARY AND CONCLUSIONS

The polarized components of fluorescence intensity observed for an oriented system containing fluorescent probe molecules were formulated, by taking into consideration a birefringence effect arising from the optical anisotropy of the polymer matrix. A method utilizing a pair of envelope curves of the polarized fluorescence intensity was established; the envelopes, which are obtained by rotating two polars synchronously in the optical apparatus for measurements, were ascertained to be useful for characterizing the molecular orientation pattern, through the model calculations. This method was applied to examine the structural transformation in the amorphous phase of nylon 6 fibres upon drawing, together with the WAXD measurements to obtain information on the crystalline domains.

The observed data of envelopes were analysed satisfactorily by using a model composed of a mixture of three orientation modes, i.e. uniaxial, three-dimensional random, and planar orientation modes, with variable parameters denoting the fractions of the respective modes. From the fractional parameters vs elongation plots, we deduced the following orientation characteristics. At an earlier stage of elongation (draw ratio ≤ 2.0), the random orientation mode was converted to the planar orientation mode as well as the uniaxial orientation mode. This implies that some non-crystalline molecules are oriented perpendicular to the draw direction, as is the long axis of the crystalline lamellae floating in the amorphous phase. On further drawing (draw ratio >2.0), the random orientation mode was no longer discernible, and the planar orientation mode induced initially was converted more and more to the highly uniaxial orientation mode. The crystalline molecular chains in the fibres exhibited a fairly high orientation state at a low draw ratio of 2.0, and further drawing caused only a small increase in the degree of molecular orientation, but was accompanied by the growth and perfection of the α-form crystals.

REFERENCES

1. Stein, R. S. and Norris, F. H., *J. Polym. Sci.*, 1956, **21**, 381.
2. Samuels, R. J., *J. Polym. Sci., Part A*, 1965, **3**, 1741.
3. Murase, S., Kudo, K. and Hirami, M., *J. Appl. Polym. Sci., Appl. Polym. Symp.*, 1991, **47**, 185.
4. Rim, P. B. and Nelson, C. J., *J. Appl. Polym. Sci.*, 1991, **42**, 1807.
5. Fu, Y., Busing, W. R., Jim, Y., Affholter, K. A. and Wunderlich, B., *Macromolecules*, 1993, **26**, 2187.
6. Roeber, S. and Zachmann, H. G., *Polymer*, 1992, **33**, 2061.
7. Lapersonne, L., Bower, D. I. and Ward, I. M., *Polymer*, 1992, **33**, 1266.
8. Hofmann, D., Goeschel, U., Walenta, E., Geiss, D. and Philipp, B., *Polymer*, 1989, **30**, 242.
9. Mutter, R., Stille, W. and Strobl, T., *J. Polym. Sci., Polym. Phys. Edn.*, 1993, **31**, 99.
10. Jawhari, T., Merino, J. C., Cabello, J. C. R. and Pastor, J. M., *Polymer*, 1992, **33**, 4199.
11. Besbes, S., Bokobza, L., Monnerie, L., Bahar, I. and Erman, B., *Polymer*, 1993, **34**, 1179.
12. Heymans, N., *J. Polym. Sci., Polym. Phys. Edn*, 1991, **29**, 1193.
13. G'Sell, C. and Lucero, A. M., *Polymer*, 1993, **34**, 2740.
14. Cansfield, D. L. M., Patel, R. and Ward, I. M., *J. Macromol. Sci.-Phys.*, 1993, **B32**, 373.
15. Kudo, K., Mochizuki, M., Kiriyama, S., Watanabe, M. and Hirami, M., *J. Appl. Polym. Sci.*, 1994, **52**, 861.
16. Clauss, B. and Salem, D. R., *Polymer*, 1992, **33**, 3193.
17. Hibi, S., Maeda, M., Kubota, H. and Miura, T., *Polymer*, 1977, **18**, 143.
18. Nishijima, Y., Onogi, Y. and Asai, T., *J. Polym. Sci., Part C*, 1966, **15**, 237.
19. Onogi, Y., Kawakami, K. and Nishijima, Y., *Kogyo Kagaku Zasshi*, 1970, **73**, 1489.
20. Nishijima, Y., *J. Polym. Sci., Part C*, 1970, **31**, 353.
21. Ward, I. M. and Hadley, D. W., *An Introduction to the Mechanical Properties of Solid Polymers*. John Wiley, London, UK, 1993, Ch. 7.
22. Nobbs, J. H. and Ward, I. M., in *Polymer Photophysics*, ed. D. Phillips. Chapman and Hall, New York, 1985.
23. Hibi, S., Fujita, K., Maeda, M., Noda, A., Suzuki, M. and Ozaki, M., *Sen-i Gakkaishi*, 1981, **37**, T-215.
24. Nishio, Y., Suzuki, H. and Sato, K., *Polymer*, 1994, **25**, 1452.
25. Nishio, Y., *PhD. Thesis*, Kyoto University, 1982.
26. Yamazaki, R., Onogi, Y. and Nishijima, Y., *Repts. Prog. Polym. Phys. Jpn.*, 1969, **12**, 439.
27. Nobbs, J. H., Bower, D. I. and Ward, I. M., *Polymer*, 1976, **17**, 25.
28. Matthes, A., *Makromol. Chem.*, 1951, **5**, 197.
29. Holmes, D. R., Bunn, C. W. and Smith, D. J., *J. Polym. Sci.*, 1955, **17**, 159.
30. Dismore, D. F. and Statton, W. O., *J. Polym. Sci., Part C*, 1966, **13**, 133.
31. Arimoto, H., Ishibashi, M., Hirai, M. and Chatani, Y., *J. Polym. Sci., Part A*, 1965, **3**, 317.
32. Bankar, V. G., Spruiell, J. E. and White, J. L., *J. Appl. Polym. Sci.*, 1977, **21**, 2341.
33. Murase, S., Kashima, M., Kudo, K. and Hirami, M., *Macromol. Chem. Phys.*, 1997, **198**, 561.
34. Kunugi, T., Yokokura, S. and Mashimoto, S., *J. Chem. Soc. Jpn*, 1976, **2**, 278.
35. Balcerzyk, E., Kozlowski, W., Wesolowska, E. and Lewaszkiewcicz, W., *J. Appl. Polym. Sci.*, 1981, **26**, 2573.
36. Katayama, K., Amano, T. and Nakamura, K., *Kolloid -Z.Z. Polym.*, 1968, **226**, 125.
37. Sakaoku, K., Morosoff, N. and Peterlin, A., *J. Polym. Sci. Polym. Phys. Edn*, 1973, **11**, 31.
38. Pinaud, F., Jarry, J. P., Sergot, Ph. and Monnerie, L., *Polymer*, 1982, **23**, 1575.